Electronic Supplementary Material (ESI) for Journal of Materials Chemistry C.

Supporting Information

Hot hole transfer from Ag nanoparticles to multiferroic YMn_2O_5 nanowires enables superior photocatalytic activity

Kazi M. Alam,[1, 2*] Sergey Gusarov,[2*] Mustafa Supur,[3] Pawan Kumar,[1] Alexander E. Kobryn,[2] Kai Cui,[2] Richard L. McCreery,[3] and Karthik Shankar[1*]

[1] Department of Electrical and Computer Engineering, University of Alberta, Edmonton, AB T6G 1H9, Canada

[2] Nanotechnology Research Centre, National Research Council Canada, 11421 Saskatchewan Drive, Edmonton, AB T6G 2M9, Canada

[3] Department of Chemistry, University of Alberta, Edmonton, Alberta T6G 2G2, Canada

*corresponding authors' email addresses: kmalam@ualberta.ca, gusarov@ualberta.ca, kshankar@ualberta.ca

[*] Tel: 780-492-1354; email: kshankar@ualberta.ca
†Electronic Supplementary Information (ESI) available. See doi:

Experimental details

Synthesis of nanostructures

Pristine mullite YMn_2O_5 nanowires were synthesized hydrothermally by invoking some modification to a previously reported recipe for fabricating $YMnO_3$.[1] Briefly, 1276 mg, 333 mg, 164 mg and 27 mg of $Y(NO_3)_3.6H_2O$, NaOH, $Mn(CH_3COO)_2.4H_2O$ and $KMnO_4$ respectively, were dissolved in 60 mL DI water, followed by continuous stirring using a magnetic stir bar at room temperature for one hour. The obtained solution was divided into three and was transferred into a Teflon-lined stainless-steel autoclave and heated for 48 hours at 170 °C. The solution was washed with methanol and DI water several times by centrifugation protocol. Finally, the obtained thick brown coloured material was dried in a vacuum oven overnight at 60 °C. The YMn_2O_5-Ag hybrid nanowires were synthesized using a previously reported Ag reduction approach.[2] Briefly, 5 mM YMn_2O_5 nanowires and 1.4 mM $AgNO_3$ (10 wt%) were added to a 10 mL solution that contained DI and ethanol (1: 4). The solution was under continuous stirring condition in an ice-bath for a few minutes. Separately, 10 mM $NaBH_4$ containing 30 mL DI solution was added drop-wise to the above solution under continuous stirring. Within a few seconds, the solution colour changed and the stirring process was stopped. The composite material in solution was washed and dried using similar protocol as pristine mullite described above. The bare Ag nanoparticles were synthesized following the same reduction mechanism.

Structural and physicochemical characterization

The fine morphological analysis of the nanostructures and elemental analysis were performed using JEOL 2200 FS transmission electron microscope (TEM) operated at 200 kV. EDX mapping was performed under STEM (scanning TEM) mode with a nominal probe size of 1 nm. The YMn_2O_5-Ag composite powders were dispersed in ultra-dilute suspensions in methanol followed

by deposition on carbon-coated copper TEM grids. The inner shell ionization edge (core loss) spectra were obtained with electron energy-loss spectroscopy (EELS), conducted under TEM imaging mode on a Hitachi H9500 TEM. The data were recorded on a Gatan GIF Tridium spectrometer. The absorption properties of pristine YMn_2O_5 nanowires, YMn_2O_5-Ag composite nanowires and pristine Ag nanoparticles in UV-Vis region were determined using a Perkin Elmer Lambda-1050 UV–Vis-NIR spectrophotometer with diffuse reflectance spectroscopy (DRS) mode. The crystalline nature and phase structure of materials were determined by X-ray powder diffractograms (XRD). The XRD spectra were acquired on a Bruker D8 advance diffractometer. This instrument uses Cu-Kα, $I\mu S\mu$ radiation (40 kV, $\lambda = 0.15418$ nm) equipped with a 2D detector (VANTEC-500). X-ray photoelectron spectroscopy (XPS) was used for the determination of chemical nature and oxidation state of the constituting elements. XPS spectra were measured using Axis-Ultra, Kratos Analytical instrument equipped with a monochromatic Al-Kα source (15 kV, 50 W; photon energy ≈1486.7 eV) operating under ultrahigh vacuum ($\sim 10^{-8}$ Torr). For the referencing the C1s peak of the adventitious hydrocarbons at ≈ 284.8 eV was used to assign the binding energy of other elements. Ultraviolet photoemission spectroscopy (UPS) was used for the determination of work functions of pristine YMn_2O_5, pristine Ag and YMn_2O_5-Ag composite. UPS spectra were also collected on the same instrument. The expression WF (ϕ) = 21.21−$E_{\text{cut-off}}$, was used for the calculation of work function, where 21.21 eV is the energy of the incident He I line of a He discharge lamp, and $E_{\text{cut-off}}$ is the cut-off energy of secondary electrons. The point of intersection by extrapolation of leading edge of graph gives the value of cut-off energy of secondary electrons $E_{\text{cut-off}}$. The value of $E_{\text{cut-off}}$ for pristine YMn_2O_5, pristine Ag and YMn_2O_5-Ag composite were found to be 16.83, 17.06 and 18.1 eV respectively, which give work function values of 4.38, 4.15 and 3.11 eV, respectively (Figure S4).

Stokes and anti-Stokes Raman spectra for pristine YMn_2O_5, YMn_2O_5-Ag composites were collected using a custom-built *f*/2 Raman spectrometer equipped with an Andor Newton 940, back-thinned charge-coupled device (CCD) detector, cooled to –80 °C.[3] Innovative Photonic Solutions (IPS) 532 nm spectrum stabilized laser module was used to generate Raman spectra. Laser output was collimated by a Thorlabs collimation package and directed to the solid sample via a 105 mm single mode fiber patch cable. Stokes and anti-Stokes Raman signals were collected employing Semrock 532 nm MaxLine laser-line filter and StopLine single-notch filter. 50 mW laser power was used on a 50 μm diameter point focus to minimize the radiation damage. Anhydrous benzonitrile was used for the routine calibration of the Raman shift axis.

Photocatalytic performance test

A Raman spectrometer (Nd:YAG laser Raman Microscope, Nicolet Omega XR) was employed to monitor the surface catalytic reduction of 4-NBT to DMAB. Dilute aqueous solutions of pristine Ag nanoparticles and YMn_2O_5-Ag composite nanowires were spin-cast at 800 rpm onto plain glass substrates followed by 30min of baking at 80 °C on a hot plate. Prior to the Raman surface catalytic experiments, an ultra-dilute solution of NBT (5×10^{-5} M) in methanol was cast onto these samples followed by vacuum drying at 60 °C. The excitation wavelength of the Raman laser was 532 nm with variable power. All Raman spectra were collected for 1 minute. The fluorescence correction factor of 6 was set prior to the data collection. The spot size was 2 μm and the confocal pinhole aperture slit was 50 μm. A $2cm^{-1}$/CCD pixel element with 900 lines mm^{-1} spectral dispersion grating was used. The Raman spectrum of DMAB was digitized from literature.[4] Spectra were acquired in air at room temperature.

Theoretical modeling and computational details

The relevant structures for DFT calculations were built based on collected X-ray powder diffractograms (XRD) and X-ray photoelectron spectroscopy (XPS) data. YMn_2O_5 (201) and Ag (111) planes were considered, where the former was constructed with oxygen vacancies. According to the high resolution XPS results in Mn2p region, there exists plenty of oxygen vacancies in synthesized mullite YMn_2O_5. This analysis (main body of the article) suggested the location of such vacancies at one tip of octahedrally coordinated Mn atom (Mn^{4+}), thus converting this to pyramidally coordinated Mn atom (Mn^{3+}). Figure S2 (a) shows the YMn_2O_5 (201) system without oxygen vacancy with the location of considered vacancy sites.

DFT calculations were performed in two steps, geometry optimization and electronic properties calculations using norm-conserving pseudopotentials,[5] and pseudo-atomic localized basis functions[6] embedded in OpenMx 3.9.2 (Open source package for Material eXplorer) package.[6] Spin-polarized calculations with periodic boundary conditions were employed for all the systems. Perdew–Burke–Ernzerhof (PBE) exchange-correlation functional has been employed within generalized gradient approximation (GGA)[7] in the DFT modeling. Scalar relativistic approach was employed in our theoretical calculations. Such approximation is computationally less demanding compared to fully relativistic approach, but still retains the main features of relativistic kinematic effects.[8] This approach is needed to account for the accurate electronic properties, particularly important for magnetic Mn atoms. We considered Hubbard U-corrections in our DFT model, where the U-value for Mn d-orbitals were considered to be 4.0 eV.[9-11] Hund's J value for Mn d-orbitals was taken as 0.88 eV.[9] For Y d-orbitals we set this U value to be 5.4 eV.[11] In the systems particularly having localized d-orbitals, electron self-repulsion results in significant error in occupation numbers and alignment of electronic levels. The Hubbard U, and Hund's J corrections

provide additional on-site Coulomb interaction and site exchange term respectively, that are needed for forcing the electrons of a particular orbital to be more localized.[12] The energy cut-off and threshold for convergence criterion for self-consistent loop was set to be 220 eV and 10^{-5} respectively. Gaussian broadening method was used to plot projected density of states (PDOS), where the broadening parameter was 0.05 eV. Electron density difference isosurface, spin density isosurface, highest occupied molecular orbital (HOMO) and lowest unoccupied molecular orbital (LUMO) were constructed using VMD (visual molecular dynamics)[13] software. The isosurface values for electron density difference and spin density were set to 0.012 eV $Å^{-3}$ and 0.03 eV $Å^{-3}$ respectively.

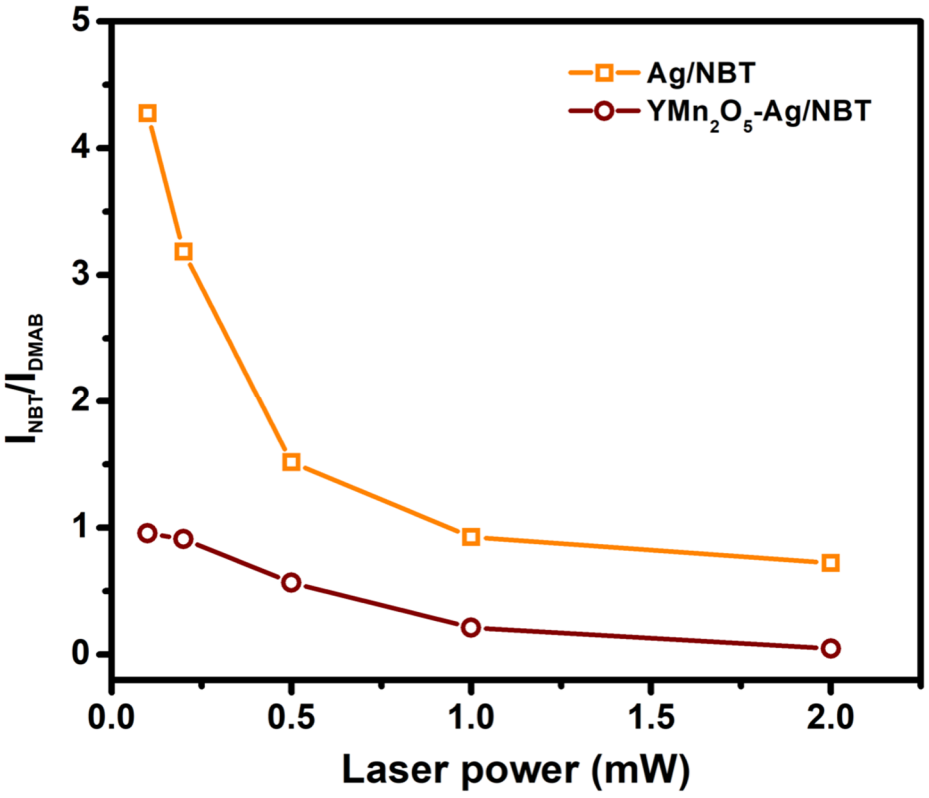

Fig. S1. Laser power dependent Raman peak intensity ratios (I_{NBT}/I_{DMAB}) of reactant (4-NBT) and product (DMAB) on pristine Ag and on YMn_2O_5-Ag hybrid. I_{NBT} was taken for 4-NBT peak at ~1332 cm^{-1} and I_{DMAB} was taken for DMAB at ~1439 cm^{-1}.

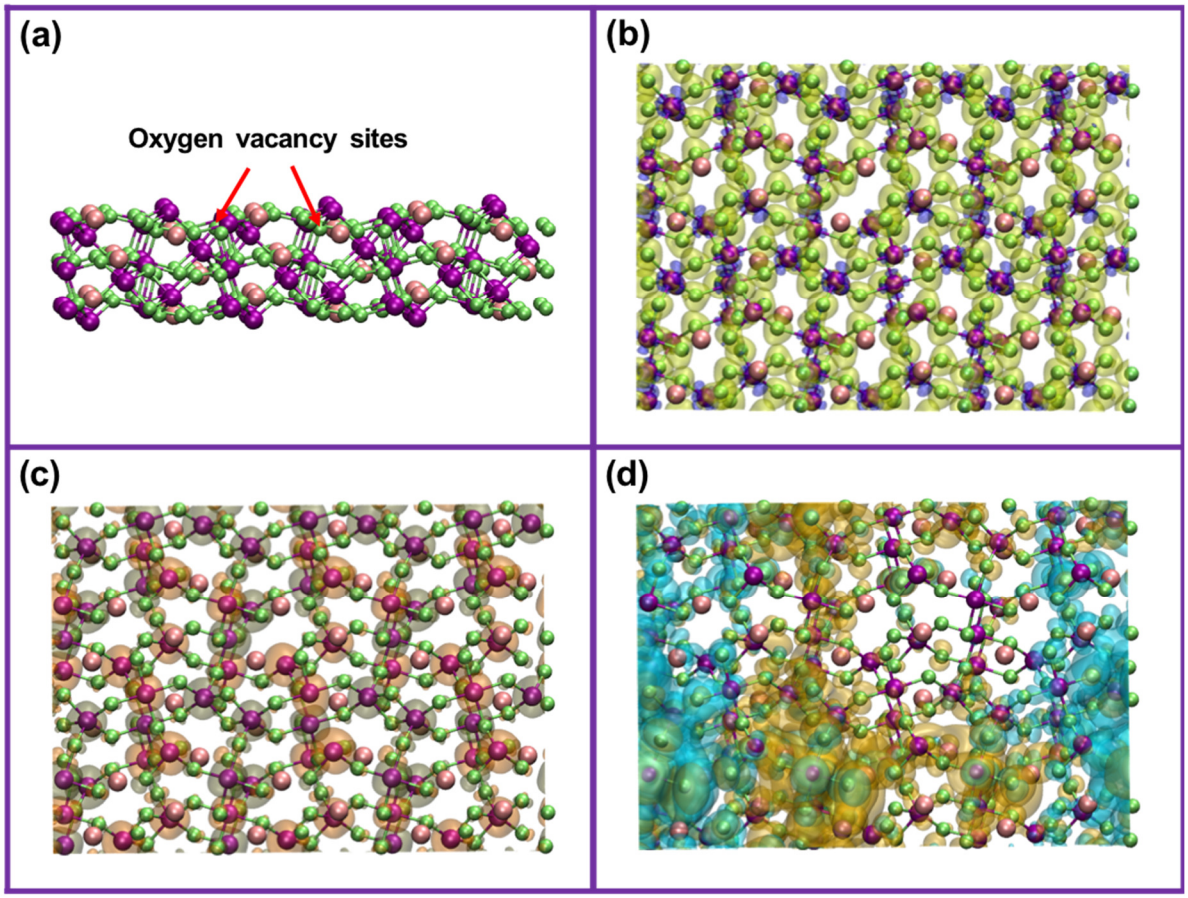

Figure S2. (a) Perspective view showing two oxygen vacancy sites of YMn_2O_5 (201). Top views showing different isosurfaces of pristineYMn_2O_5 (201); (b) electron density difference where the transparent blue and yellow surfaces represent charge depletion and accumulation regions respectively (the isosurface value is set to 0.012 eV $Å^{-3}$), (c) spin density difference where the transparent olive and orange surfaces represent spin-up and spin-down electron dominated regions respectively (the isosurface value is set to 0.03 eV $Å^{-3}$) and (d) spatial distributions of molecular orbitals where the transparent cyan and gold surfaces represent highest occupied molecular orbital (HOMO) and lowest unoccupied molecular orbital (LUMO) respectively. Pink, purple, lime and silver colours are for Y, Mn, O and Ag atoms respectively.

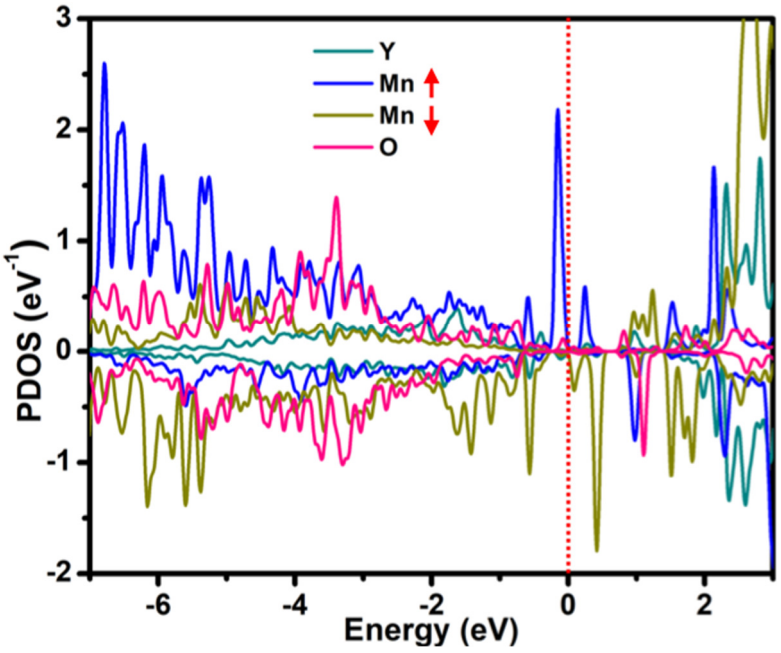

Figure. S3. Projected density of states (PDOS) of Y, Mn and O atoms of pristine YMn_2O_5 (201). The red arrows indicate two opposite spin dominated Mn atoms. The red dotted line indicates the Fermi level.

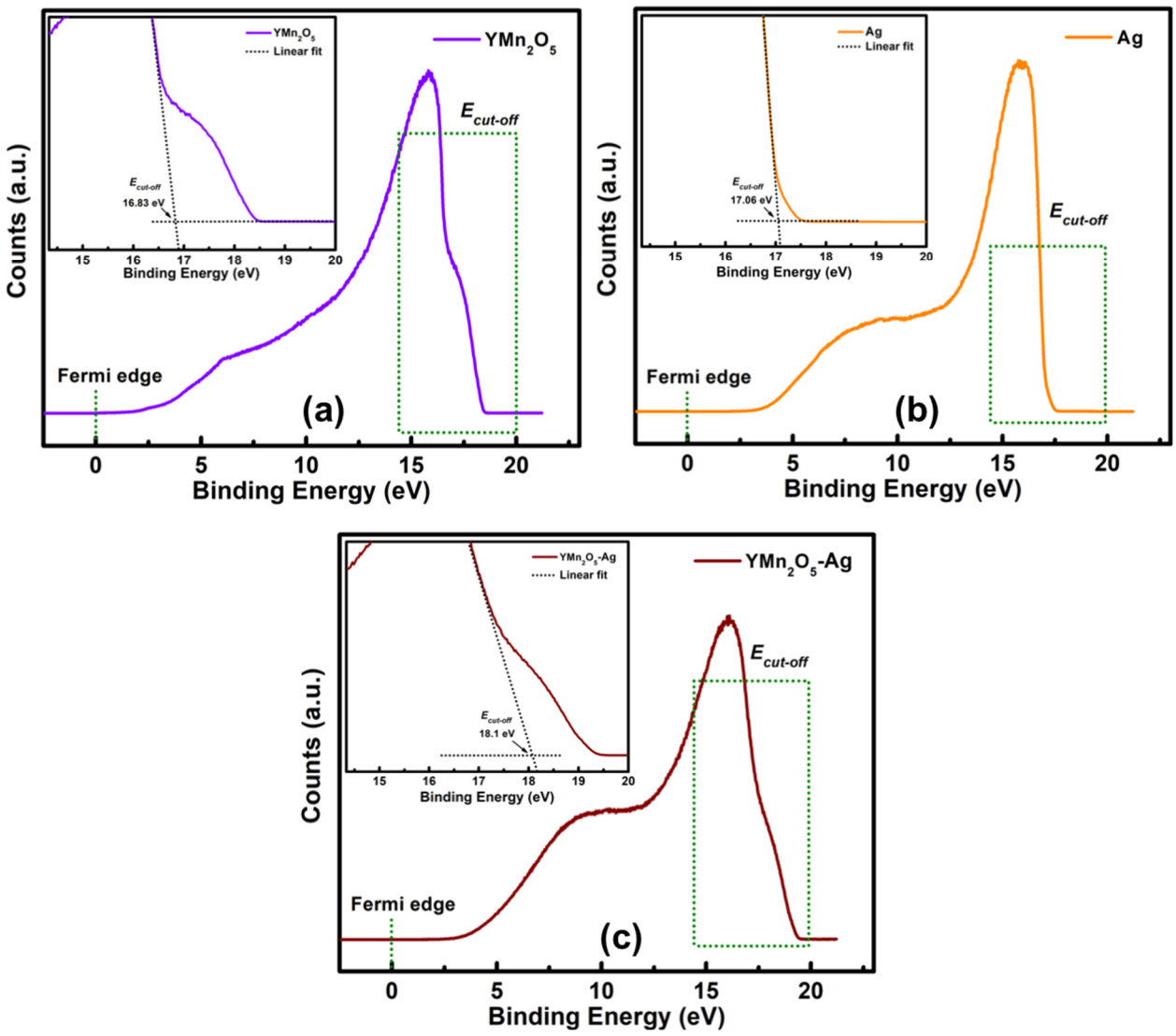

Figure S4. (a) UPS work function of (a) pristine YMn_2O_5 nanowires, (b) pristine Ag nanoparticles, (c) YMn_2O_5-Ag hybrid nanowires.

References

1. Dhinesh Kumar, R.; Jayavel, R., Low temperature hydrothermal synthesis and magnetic studies of YMnO3 nanorods. *Materials Letters* **2013,** *113*, 210-213.
2. Mohan, S.; Subramanian, B.; Sarveswaran, G., A prototypical development of plasmonic multiferroic bismuth ferrite particulate and fiber nanostructures and their remarkable photocatalytic activity under sunlight. *J. Mater. Chem. C* **2014,** *2* (33), 6835-6842.
3. Supur, M.; Smith, S. R.; McCreery, R. L., Characterization of Growth Patterns of Nanoscale Organic Films on Carbon Electrodes by Surface Enhanced Raman Spectroscopy. *Anal Chem* **2017,** *89* (12), 6463-6471.
4. You, T.; Jiang, L.; Yin, P.; Shang, Y.; Zhang, D.; Guo, L.; Yang, S., Direct observation ofp,p′-dimercaptoazobenzene produced fromp-aminothiophenol andp-nitrothiophenol on Cu2O nanoparticles by surface-enhanced Raman spectroscopy. *Journal of Raman Spectroscopy* **2014,** *45* (1), 7-14.
5. Bachelet, G. B.; Hamann, D. R.; Schlüter, M., Pseudopotentials that work: From H to Pu. *Physical Review B* **1982,** *26* (8), 4199-4228.
6. Ozaki, T., Variationally optimized atomic orbitals for large-scale electronic structures. *Physical Review B* **2003,** *67* (15), 155108-5.
7. John P. Perdew, K. B., Matthias Ernzerhof, Generalized gradient approximation made simple. *PHYSICAL REVIEW LETTERS* **1996,** *77* (18), 3865-3868.
8. Koelling, D. D.; Harmon, B. N., A technique for relativistic spin-polarised calculations. *Journal of Physics C: Solid State Physics* **1977,** *10* (16), 3107-3114.
9. Partzsch, S.; Wilkins, S. B.; Hill, J. P.; Schierle, E.; Weschke, E.; Souptel, D.; Buchner, B.; Geck, J., Observation of electronic ferroelectric polarization in multiferroic YMn2O5. *Phys Rev Lett* **2011,** *107* (5), 057201.
10. Giovannetti, G.; van den Brink, J., Electronic correlations decimate the ferroelectric polarization of multiferroic homn2o5. *Phys Rev Lett* **2008,** *100* (22), 227603.
11. Li, C.; Thampy, S.; Zheng, Y.; Kweun, J. M.; Ren, Y.; Chan, J. Y.; Kim, H.; Cho, M.; Kim, Y. Y.; Hsu, J. W.; Cho, K., Thermal stability of mullite RMn(2)O(5) (R = Bi, Y, Pr, Sm or Gd): combined density functional theory and experimental study. *J Phys Condens Matter* **2016,** *28* (12), 125602.
12. Capdevila-Cortada, M.; Łodziana, Z.; López, N., Performance of DFT+U Approaches in the Study of Catalytic Materials. *ACS Catalysis* **2016,** *6* (12), 8370-8379.
13. Humphrey, W.; Dalke, A.; Schulten, K., VMD: Visual molecular dynamics. *Journal of Molecular Graphics* **1996,** *14* (1), 33-38.